Journal of Solid State Chemistry **147,** 26–37 (1999)
Article ID jssc.1999.8140, available online at http://www.idealibrary.com on IDEAL®

# What Determines the Structures of the Group 15 Elements?[1]

Dong-Kyun Seo and Roald Hoffmann[2]

*Department of Chemistry and Cornell Center of Materials Research, Cornell University, Ithaca, New York 14853-1301*

Received August 5, 1998; in revised form November 25, 1998; accepted December 11, 1998

**The structures of black phosphorus (orthorhombic), As, Sb, and Bi (rhombohedral) have been traditionally interpreted as resulting from a Peierls distortion from an ideal simple cubic structure. We examine this idea in detail by calculating the Fermi surfaces of simple cubic phosphorus with the extended Hückel tight-binding method and by looking at some simpler models to understand the trends. The calculated Fermi surfaces for cubic P are *not* nested, which argues strongly that the structural distortion in black phosphorus has little to do with Peierls instability. Within the (simple) Hückel approximation for *p*-orbital interactions, the Fermi surface nesting is still perfect, even when interchain ($\pi$-type) interactions are included. Next-nearest-neighbor interaction and *s–p* mixing completely destroy the Fermi surface nesting. The observed strong *s–p* mixing implies that it is just this mixing that causes the deformation to the highly stable black phosphorus structure, forming lone pairs in the process. We suggest that in order to understand the trend in the magnitude of distortions in the structures of the group 15 elements (P > As > Sb > Bi) *s–p* mixing should not be neglected even in the heavier elements.** © 1999 Academic Press

***Key Words:*** **group 15 elements; band structure calculations; structural distortions; *s–p* mixing; Peierls distortion; Fermi surface nesting.**

## INTRODUCTION

One-dimensional (1D) solids with partially filled bands have an innate tendency to lower their electronic energy by opening a band gap at the Fermi level (1–3); the band gap opening leads to structural modulation, which is referred to as a charge density wave (CDW) (4–9). This electronic instability is called a "CDW instability" or "Peierls instability." The effect is analogous to the first-order Jahn–Teller instability of a molecule, i.e., the tendency of a molecule with partially filled degenerate HOMO's to undergo a symmetry-lowering distortion which splits the degenerate level into the filled and empty ones, opening an energy gap between the two (5, 6). The structural distortion driven by the Peierls instability is called a "Peierls distortion" (5, 6, 10), analogous to a Jahn–Teller distortion (11).

Peierls instabilities are often discussed in terms of Fermi surface nesting (4–6). It is the nested portion of the Fermi surfaces that is responsible for the distortion and disappears after the distortion. The nesting vector **q** is directly related to the unit cell length of the modulated structure. It has been proven that the metals with isotropic Fermi surfaces (such as a Fermi sphere) cannot have a Peierls instability (8). Thus, the topology of Fermi surface is important in studying CDW materials. Indeed, Fermi surface calculations have proven indispensable in the field (4–9).

A CDW phenomenon also occurs in certain two-dimensional metals, although their Fermi surface seems to exhibit no nesting. This led to the development of the concept of hidden Fermi surface nesting: the combined Fermi surfaces of such a system are decomposed into a set of hidden 1D Fermi surfaces, and the nesting associated with the hidden surfaces is responsible for the observed geometrical distortions (5, 6).

The structural modulation in materials driven by the Peierls instability is accompanied by a metal-to-semiconductor or metal-to-insulator transition (5, 7–9, 12). This is due to the fact that the modulation diminishes the density of state (DOS) at the Fermi level (13). The resultant structural distortion is thus clearly distinguishable from other deformations in terms of both its origin (Fermi surface nesting) and the anomalous changes in the physical properties. Sometimes, the structural modulation of a metal can originate from the lowering of the energy levels lying well below the Fermi level. The situation is then analogous to a molecule with no partially filled degenerate HOMO's, yet which can nevertheless undergo a symmetry-lowering distortion, a phenomenon typically described as a second-order Jahn–Teller instability (2). This distortion may (or may not) induce a band gap opening. It has been noted that this type of modulation should not be considered as a Peierls distortion in a strict sense (14).

Black phosphorus, As, Sb, and Bi, have layered structures in which each atom has three short bonds in the layer and

[1]This paper is dedicated to the memory of Jean Rouxel.

[2]To whom correspondence should be addressed. E-mail: rh34@cornell.edu.



0022-4596/99 $30.00

relatively long contacts with the atoms in the neighboring layer (15, 16). Black phosphorus has an orthorhombic (A17) structure (Fig. 1) and is semiconducting, while the semimetals, As, Sb, and Bi, possess a rhombohedral (A7) structure (Fig. 2). Though highly distorted, in distinct ways, both structures are related to a simple cubic structure, as shown schematically in Fig. 3. Going down group 15, the distances between adjacent atoms within a layer and between layers differ less, so that the coordination environment surrounding an atom deviates less from a regular octahedron. A "weaker" structural instability as we go down the group is implied. This can be seen also in studies of these materials under high pressure; black phosphorus is found to transform (reversibly) to a simple cubic structure at much higher pressure ( $\sim$12 GPa) than the pressure ( $\sim$5 GPa) at which As does (17). Both elements are metallic in their simple cubic form (15, 16, 18).

The idea of Peierls distortion has been employed to explain the structural trends in the group 15 elements (10, 19–23). Both A7 and A17 structural types can be derived from a simple cubic lattice by breaking three linkages and keeping the other three around each site (see Fig. 3). For the simple cubic phases of As, Sb, and Bi, Cohen *et al.* argued that the electronic configuration responsible for bonding is $p^3$, which gives rise to three $p$ bonds at right angles and octahedral coordination (24). This is due to the fact that the **s** electrons, lying deeper, tend to participate much less in the chemical bonding in heavy elements (25). Littlewood explained the A7 structure of As, Sb, and Bi as a consequence of the Peierls instability inherent in a simple cubic phase with half-filled $p$ bands (19, 20). In addition, he considered $s$–$p$ mixing to be more important in forming the A17 structure of black phosphorus.

A more detailed analysis of these systems (using band concepts) was carried out by Burdett and Lee (10). They considered for simplicity only the $\sigma$-type $p$-orbital ($p_\sigma$) interaction within the Hückel approximation, and showed that the structures of black phosphorus, As, Sb, and Bi can be derived by Peierls distortion from the ideal simple cubic structure. With the $p^3$ electron configuration, *all* the group 15 elements possess three independent half-filled $p$ bands, each from one of three orthogonal $p$ orbitals, that is, $p_x$, $p_y$ and $p_z$. By analogy with the 1D case, we should expect a distortion away from simple cubic by fission of alternate linkages along $x$, $y$, and $z$ directions.

As Burdett and Lee already noted in their paper, however, the simple idea described above is not of much use in tracing the origin of the structural distortion. When the $s$–$p$ mixing is strong, the $s^2p^3$ electron configuration of the group 15 elements results in a three-coordinate solid with a lone pair occupying one coordination position. This also can explain the structural distortions in the group 15 elements. The $s$–$p$ mixing is a local effect and is not obviously related to bands, or, the Peierls instability. Gaspard *et al.*'s recent work on amorphous and liquid phases of the group 15 elements also shows that the long-range order of the materials does not play a role in the bonding mechanism (26).

We thought it important to examine systematically the origin of structural distortions in the group 15 elements. As a representative example we choose the simple cubic P structure. We begin our analysis with reconsidering Burdett and Lee's argument in terms of the Fermi surface nesting. Next, we show how this simple picture gradually changes and becomes complicated when additional interactions are included. Finally, we calculate its Fermi surfaces

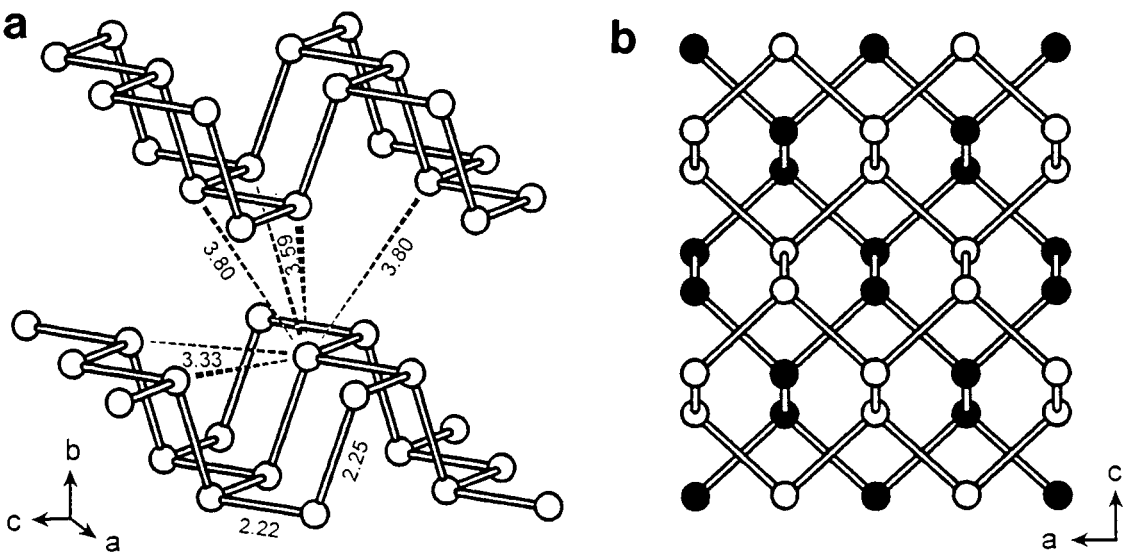


**FIG. 1.** The black phosphorus (A17) structure (a) in a perspective view and (b) in a projection on **ac** plane. In the projection, the circles of P atoms in the lower layer are filled. The P–P distances are given in Å (Ref. (15a)).

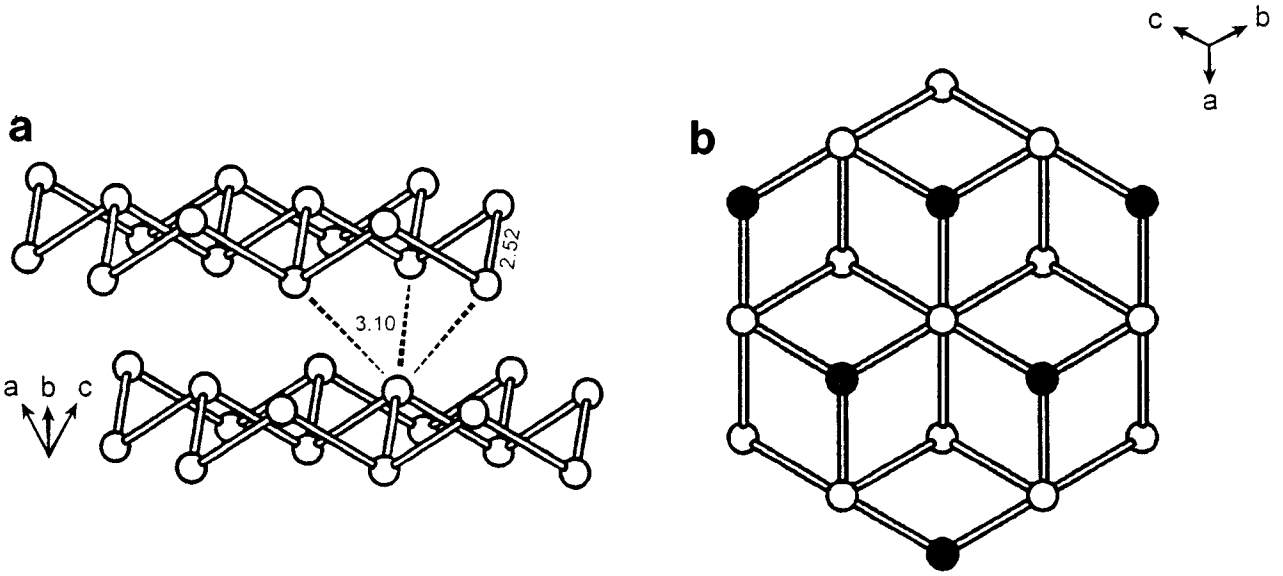


**FIG. 2.** The As (A7) structure (a) in a perspective view and (b) in a projection along $\mathbf{a} + \mathbf{b} + \mathbf{c}$ direction. In the projection, the circles of As atoms in the lower layer are filled. The top atoms in the upper layer overlap perfectly with the bottom atoms in the lower layer. The As–As distances are given in Å (Ref. (15b)).

employing the extended Hückel tight-binding method (27, 28). All the calculations were carried out using the CAESAR program (29). The unit-cell length of the simple cubic P structure is chosen to be 2.38 Å from the literature (16, 18a). A weighted $H_{ij}$ formula was used for the extended Hückel calculations, and for all the calculations the following atomic parameters were employed ($H_{ii}$ = orbital energy, $\zeta$ = Slater exponent): P3*s*, −18.9 eV, 1.881; 3*p*, −10.6 eV, 1.629 (30).

## $p_\sigma$ INTERACTION WITHIN THE HÜCKEL APPROXIMATION

We begin with a Hückel model analysis, and $p$–$p$ $\sigma$ interactions only. In a simple cubic cell **1a**

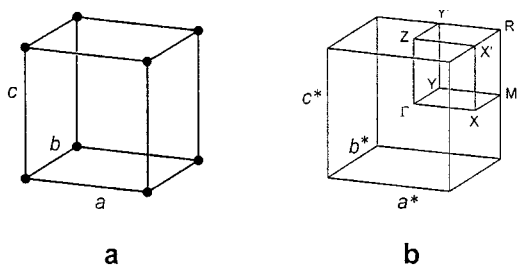


**Scheme 1**

with a unit cell length a, the three orthogonal $p$-orbitals, $p_x$, $p_y$, and $p_z$, generate bands with energies (10),

$$p_x, \quad \varepsilon(\mathbf{k}) = \alpha + 2\beta_\sigma \cos k_x a$$

$$p_y, \quad \varepsilon(\mathbf{k}) = \alpha + 2\beta_\sigma \cos k_y a$$

$$p_z, \quad \varepsilon(\mathbf{k}) = \alpha + 2\beta_\sigma \cos k_z a,$$

where $\alpha$ and $\beta_\sigma$ ( $> 0$) are the Coulomb and $p$–$p$ $\sigma$ resonance integrals, and $\mathbf{k}$ is a three-dimensional wave vector, $\mathbf{k_x} + \mathbf{k_y} + \mathbf{k_z}$ or ($k_x/a^*$, $k_y/b^*$, $k_z/c^*$) (Fig. 4). The $\mathbf{k}$'s are in the range of $-\pi/a < k_x, k_y, k_z \leq \pi/a$. This first Brillouin zone (FBZ) is drawn in Scheme 1b. For the $p^3$ configuration, all the three bands are half-filled. The Fermi level $\varepsilon(\mathbf{k_F}) = \alpha$ cuts halfway through all the dispersion curves connecting two special $\mathbf{k}$ points in Fig. 4.

A Fermi surface is defined as a collection of the Fermi vectors, $\mathbf{k_F}$'s, in the FBZ. In Scheme 2a,

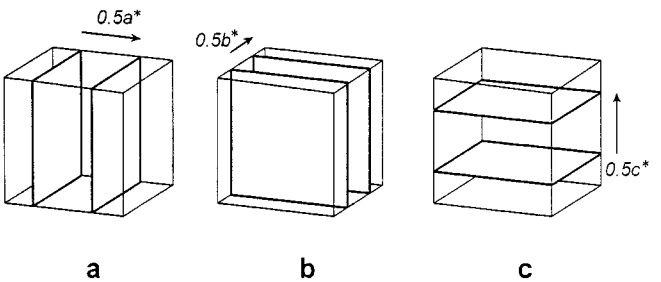


**Scheme 2**

the 1D Fermi surface arising from the $p_x$ band is then given by two parallel planes, i.e., ($\pm 0.25$, $y$, $z$), perpendicular to the line $\Gamma \rightarrow X$. The Fermi surface divides the FBZ into three regions; the middle region is empty of electrons while the other two are occupied. We can see that the Fermi surface is perfectly nested with a nesting vector $\mathbf{q_a} = 0.5\mathbf{a}^*$.

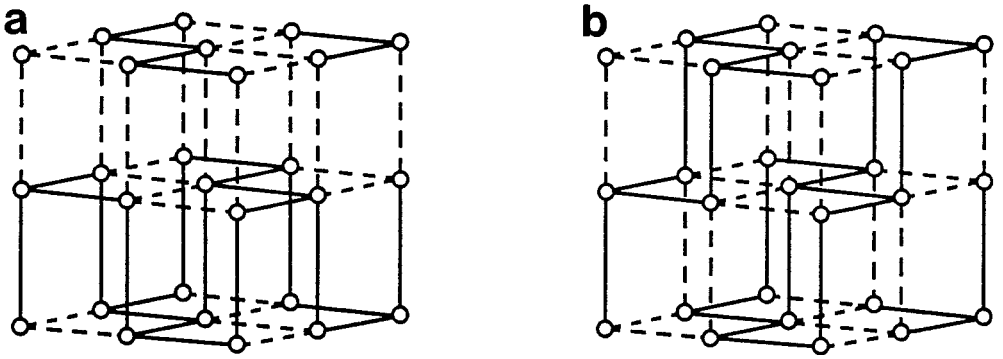


**FIG. 3.** Schematic diagrams of (a) black phosphorus and (b) As structures displaying their relation to a simple cubic structure. Solid and broken lines denote intra- and interlayer atom distances, respectively. (adapted from Ref. (10).

This Fermi surface nesting will be responsible for the fission of alternate linkages along the $x$ direction. Likewise, the $p_y$ and $p_z$ bands give rise to perfectly nested 1D Fermi surfaces with nesting vectors $\mathbf{q}_b = 0.5\mathbf{b}^*$ and $\mathbf{q}_c = 0.5\mathbf{c}^*$, respectively (Schemes 2b and 2c). The same type of bond alternation as along $x$ should occur also along $y$ and $z$. The combined Fermi surfaces of 2a to 2c are shown in Scheme 3.

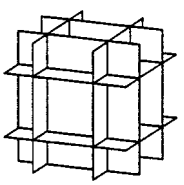

**Scheme 3**

The combined Fermi surfaces **3** can be divided in a different way, regardless of the origin of each set of the Fermi surfaces. This (hidden Fermi surface nesting) idea is based upon assignment of the bands, not by their origin in $p_x$, $p_y$, $p_z$ but in order of energy at each **k** point (Fig. 4). So, the band with the lowest energy is labeled with 1, and the highest one with 3. In the FBZ, band 1, the lowest band, is all occupied except around Γ, resulting in a cube-shaped *hole* pocket centered at Γ (**4a**).

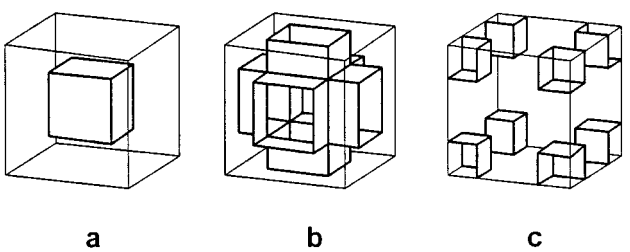


**Scheme 4**

On the other hand, an *electron* pocket of the same shape is formed around R (**4c**) from the highest, mostly unoccupied band 3. A cross made of three perpendicular squared pipes is centered at Γ, originating from band 2 (**4b**). The outside of the cross is occupied by electrons. It can be easily seen that the combination of **4a** to **c** gives rise to **3**, i.e., the combination of the three pairs of 1D Fermi surfaces (**2a** to **c**). The edges and corners of **4a** to **c** correspond to the **k** point sets shared by two and three of these 1D Fermi surfaces, respectively. This implies that at the **k** points on those edges and corners the bands are doubly and triply degenerate, respectively. As we shall see later, these degeneracies can be lifted easily by some additional interactions. In that case, the Fermi surfaces of **4a** to **c** may not share their edges or corners any longer, and their combination does not produce perfect 1D Fermi surfaces but shows fragmentation of them. In other words, the additional interactions may cause the $p_x$, $p_y$, and $p_z$ orbitals to mix together, destroying the independent well-nested 1D nature of the $p_x$, $p_y$, and $p_z$ bands.

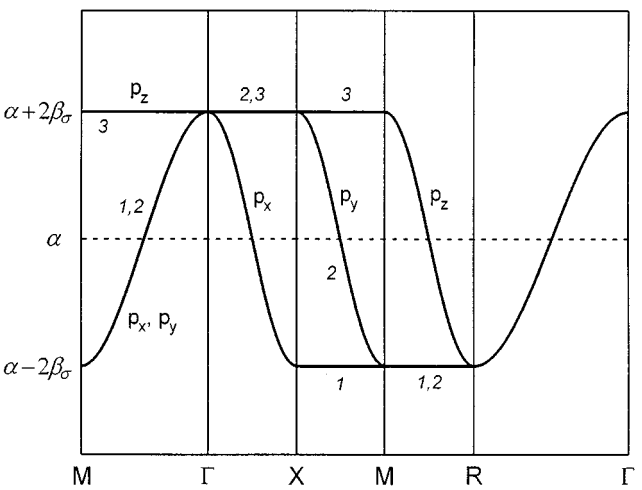


**FIG. 4.** Schematic dispersion relations of the bands of a simple cubic structure with $p$ orbitals, considering the $p_\sigma$ interaction within the Hückel approximation. The dashed line refers to a Fermi level with a $p^3$ electron configuration. Γ = (0, 0, 0), $X$ = (0.5, 0, 0), $M$ = (0.5, 0.5, 0), and $R$ = (0.5, 0.5, 0.5).

## $p_\sigma$ AND $p_\pi$ INTERACTIONS WITHIN THE HÜCKEL APPROXIMATION

If $p$–$p$ π interactions are included, the energy dispersion relations become

$$p_x, \quad \varepsilon(\mathbf{k}) = \alpha + 2\beta_\sigma \cos k_x a + 2\beta_\pi \cos k_y a + 2\beta_\pi \cos k_z a$$

$$p_y, \quad \varepsilon(\mathbf{k}) = \alpha + 2\beta_\pi \cos k_x a + 2\beta_\sigma \cos k_y a + 2\beta_\pi \cos k_z a$$

$$p_z, \quad \varepsilon(\mathbf{k}) = \alpha + 2\beta_\pi \cos k_x a + 2\beta_\pi \cos k_y a + 2\beta_\sigma \cos k_z a$$

where $\beta_\pi$ ($< 0$; $|\beta_\pi| < |\beta_\sigma|$) is the $p$–$p$ π resonance integral. We need an estimate of $\beta_\sigma$ and $\beta_\pi$; these were obtained by calculating the overlap integrals between $p$ orbitals of the nearest neighbors and using the Wolfsberg–Helmholz formula (27). In this way we obtain $\beta_\sigma = 6.02$ eV, $\beta_\pi = -2.16$ eV. The resulting band structure is presented in Fig. 5; with the Fermi level $\alpha = -10.6$ eV. The additional $p_\pi$ interaction actually changes the band structure quite a lot. The three crystal orbitals degenerate at Γ are stabilized due to their π bonding character. The previously nondispersive curves in Fig. 4 now run up as π antibonding increases when **k** departs from Γ. The crystal orbitals at $R$ have the most π antibonding character. In Fig. 5, the **k** points cut by the Fermi-level are not always halfway between two special **k** points, implying that the Fermi surfaces are no longer perfectly flat.

The Fermi surfaces associated with these bands are presented in Fig. 6a as cross-sections in the planes $k_z = 0$ and $0.5\mathbf{c}^*$ and in Fig. 6b as a perspective stereoview. As expected from the band structure in Fig. 5, the Fermi surface from each band consists of two strongly wraped sheets perpendicular to the sheets from the other two bands. Although their shapes deviate significantly from the perfect 1D Fermi surfaces, the following simple mathematical reasoning reveals that perfect nesting still occurs between each pair of these quasi 1D Fermi surfaces, through a common nesting vector, $\mathbf{q} = 0.5\mathbf{a}^* + 0.5\mathbf{b}^* + 0.5\mathbf{c}^*$. Consider, for example, the $p_x$ band and its Fermi surfaces. At any $\mathbf{k}_F$ on this Fermi surface, $2\beta_\sigma \cos k_x a + 2\beta_\pi \cos k_y a + 2\beta_\pi \cos k_z a$ will be 0, since $\varepsilon(\mathbf{k}_F) = \alpha$. For this $\mathbf{k}_F$ to be nested by **q**, there should exist a corresponding Fermi vector, $\mathbf{k}_F + \mathbf{q}$. This condition is satisfied owing to the fact that $2\beta_\sigma \cos(k_x a + \pi) + 2\beta_\pi \cos(k_y a + \pi) + 2\beta_\pi \cos(k_z a + \pi) = -(2\beta_\sigma \cos k_x a + 2\beta_\pi \cos k_y a + 2\beta_\pi \cos k_z a) = 0$. The same logic holds for the $p_y$ and $p_z$ bands as well.

The perfect Fermi surface nesting found in Fig. 6 indicates that the Peierls instability should occur, even when interchain ($p_\pi$) interactions exist. The observed common nesting vector, $\mathbf{q} = 0.5\mathbf{a}^* + 0.5\mathbf{b}^* + 0.5\mathbf{c}^*$, implies that unit-cell doubling should occur along all three directions *simultaneously*. However, the actual magnitude of the distortion is expected to be smaller than in the absence of interchain interactions. This is because the driving force for the Peierls instability is weakened when the nested $\mathbf{k}_F$'s are located away from the halfway point along the direction of the distortion in the FBZ. A simple example illustrating this is a pair of hypothetical linear hydrogen chains along the **a** direction, interacting perpendicular to each other (31). As interchain interactions become stronger, the Fermi vectors lie farther from $\pm 0.25\mathbf{a}^*$, thereby leading to a weaker Peierls instability (31c).

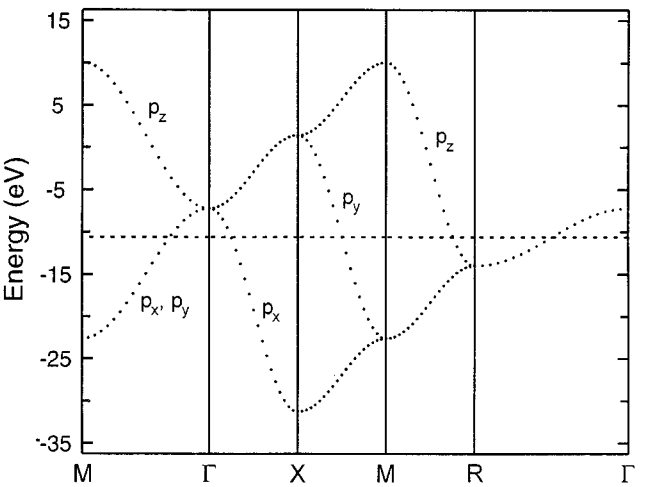


**FIG. 5.** Dispersion relations of the bands of the simple cubic P structure, calculated only with $p$ orbitals and considering the $p_\sigma$ and $p_\pi$ interactions within the Hückel approximation. The calculated $\beta_\sigma$ and $\beta_\pi$ are 6.02 and $-2.16$ eV, respectively. The dashed line refers to a Fermi level for a $p^3$ electron configuration.

## EXTENDED HÜCKEL CALCULATION ONLY WITH $p$ ORBITALS

As one moves from simple to extended Hückel calculations, inclusion of overlap integrals destabilizes the antibonding part of a band. In comparison with Fig. 5, the upper (antibonding) part of the bands in Fig. 7 is much raised, so that the Fermi level lies nearer the bottom of the bands. Long-range (especially, next-nearest-neighbor) interactions lift the degeneracy at the low-symmetry **k** points along $\Gamma \rightarrow M$ and $\Gamma \rightarrow R$. Along $\Gamma \rightarrow M$, the low symmetry allows a mixing between the $p_x$ and $p_y$ orbitals, generating two bands, each from a linear combination $\sim p_x + p_y$ or $\sim p_x - p_y$. Schemes 5a and 5b depict (in projection) the linear combinations at Γ and $M$ resulting from the $p_x + p_y$ and $p_x - p_y$ bands, respectively (32).

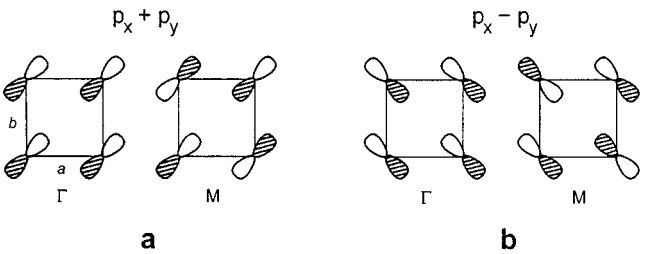


**Scheme 5**

At Γ or $M$, they have the same energies, being equivalent in σ- and π-type interactions along the face-diagonal directions. The σ-type interaction destabilizes these crystal orbitals both at Γ and $M$, while the opposite holds for the π-type interaction. This degeneracy no longer holds at **k** points between Γ and $M$. On going away from Γ or $M$, the σ antibonding turns into bonding, while the π bonding turns into antibonding. Clearly the $p_x + p_y$ band will change in energy more than the $p_x - p_y$ band along this line, due to its σ-type interaction along the **a** + **b** direction. At the halfway point, (0.25, 0.25, 0), the interactions are maximized, resulting in the largest energy difference between the two bands.

The same effect is responsible for the degeneracy lifting along $\Gamma \rightarrow R$. The symmetry imposed at the **k** points along $\Gamma \rightarrow R$ allows the three $p$ orbitals to participate equivalently in the face-diagonal interactions along **a** + **b**, **b** + **c**, and **c** + **a**. Thus, there is a linear combination, $\sim p_x + p_y + p_z$, pointing along **a** + **b** + **c**, a body-diagonal direction. The other two linear combinations are orthogonal to it. The linear combination $p_x + p_y + p_z$ at Γ and $R$ is shown in Scheme 6.

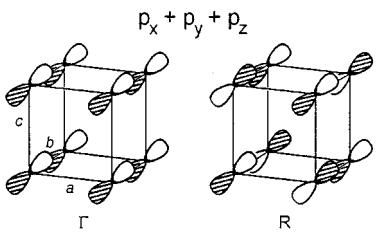


**Scheme 6**

The orbitals at the next-nearest-neighbor sites interact with each other in an antibonding manner. As in the case of $\Gamma \rightarrow M$, the character of the interaction changes and becomes more bonding on going away from Γ or $R$. At halfway points, the energy splitting is larger along $\Gamma \rightarrow R$ than along $\Gamma \rightarrow M$. This is expected, since the former direction allows more orbitals to interact than the latter does.

The band splitting described above actually occurs throughout the entire FBZ. This is important, because the bands involved here are the ones cut by the Fermi level. We expect large changes in the shapes of the Fermi surfaces due to the band splitting. The Fermi surfaces associated with these bands are presented in Fig. 8a as cross-sections in the planes of $k_z = 0$ and 0.5**c*** and in Fig. 8b in a perspective stereoview. The overall features of these surfaces may be analyzed by thinking about their connection to the simplified Fermi surfaces, **4a** to **4c**. The hole pocket from the lowest band gives a Fermi surface in shape of a rounded cube centered at Γ. The second Fermi surface has the shape of a cross made of three perpendicular square-like cylinders. The highest band leads to an electron pocket in the shape of a small rounded cube and centered at $R$ with eight spikes at the corners. The spikes point toward Γ and connect this third Fermi surface to the cross.

Clearly these Fermi surfaces are *not* well nested, and at best the nesting appears only between the walls facing each other in the cross. Comparing to the Fermi surfaces of **4a** to **4c**, we may conclude that the nesting does not occur here because the two cubes are too small to align their faces with the walls of the cross in Fig. 8. It is the band-splitting that makes these cubes diminish. In turn, the band-splitting results from the long-range interactions between the $p$ orbitals.

## BAND STRUCTURE OF SIMPLE CUBIC P

Figure 9 shows the dispersion relations of a simple cubic phosphorus structure, calculated with the extended Hückel tight-binding method. Now $s$ orbitals are included. Overall, the main features of the band structure are in good agreement with those from other calculations (23). The compositions of the crystal orbitals at the special **k** points are also given in Fig. 9. The lowest band has mainly $s$ character, except around $M$ and $R$. The $s$ orbitals interact sufficiently strongly, so that the $s$ band actually overlaps with the high-lying $p$ bands. At the low-symmetry **k** points, the $s$ and $p$ orbitals mix together.

The interaction between $s$ and $p$ bands has a dramatic effect on the band structure near $R$. At $R$ the crystal orbital of $s$ character is most destabilized, as a consequence of antibonding along all three unit-cell vector directions. The corresponding crystal orbitals of $p$ character are, however, stabilized by $p$–$p$ σ bonding. Thus, the highest $p$ band changes its orbital character to $s$ on going from $M$ or Γ to $R$. The band crossing between the $s$ and $p$ bands is avoided, due to the low symmetry of the **k** points in between. This results in strong band repulsion, especially along $\Gamma \rightarrow R$. Crystal orbitals of the $s$ band interact with those of the $p_x + p_y$ and $p_x + p_y + p_z$ linear combinations along $\Gamma \rightarrow M$ and $\Gamma \rightarrow R$, respectively. Note that this has nothing to do with long-range interactions. The $s$–$p$ mixing occurs largely through the nearest-neighbor $s$–$p$ interactions along each unit-cell vector direction. In the symmetry that is present along $\Gamma \rightarrow R$, the $s$ orbitals undulate in the same way along **a**, **b**, and **c** directions. Only the $p_x + p_y + p_z$ linear combination has the same symmetry for the interaction. Likewise, it is the $p_x + p_y$ linear combination that matches the $s$ combination along $\Gamma \rightarrow M$.

The $s$–$p$ mixing we observe is important, because the band repulsion resulting from it changes the highest band significantly. This band is always kept above the Fermi level, and is now no longer cut by the Fermi level. We expect only two sets of Fermi surfaces from the band structure. For the two lower $p$ bands, the $s$–$p$ mixing may not affect their Fermi surfaces as significantly as in the case of the highest band. However, it should be noted that now the filled region of

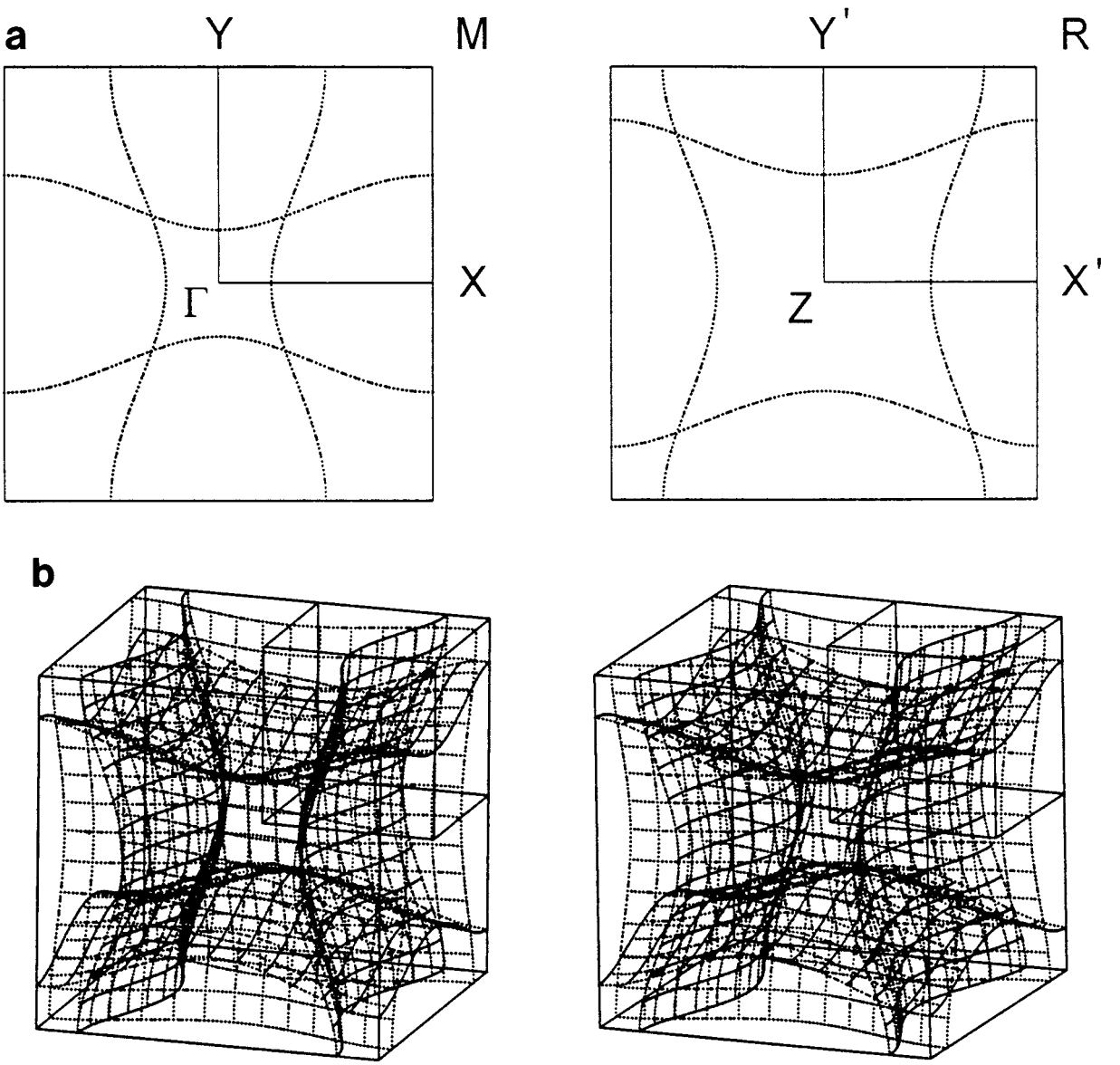


**FIG. 6.** The Fermi surfaces from the band structure of Fig. 5 in (a) cross-section views on the planes of $k_z = 0$ and 0.5**c*** and in (b) a perspective stereoview. $Y = (0, 0.5, 0)$, $Z = (0, 0, 0.5)$, $X' = (0.5, 0, 0.5)$, and $Y' = (0, 0.5, 0.5)$.

those *p* bands has a large antibonding contribution from the *s*–*p* interactions. This is reflected in the raised Fermi level in Fig. 9, compared to that in Fig. 7.

The Fermi surfaces associated with these bands are presented in Fig. 10a as cross-sections in the planes of $k_z = 0$ and 0.5**c***, and in Fig. 10b as a perspective stereoview. They are in good agreement with those calculated by other methods (23). As expected, there occur only two Fermi surfaces in Fig. 10. A sphere-like hole pocket centered at Γ is from the second energy curve in Fig. 10, while the third energy curve creates a cross of three nearly circular pipes. The size of the cross is larger and its shape is more regular in our calculation than in other work (23). This difference may be mainly due to the slightly exaggerated *s* orbital interactions in our calculation. The two Fermi surfaces merge together at eight points located along the body-diagonal directions. The small electron pocket in Fig. 8 now disappears.

It is clear that the Fermi surface nesting does not occur in this structure. Thus, the Peierls instability is not inherent in the electronic structure of simple cubic P. It is interesting to notice that the shapes of the Fermi surfaces in Fig. 10 are quite similar to those of $ReO_3$, a transition metal oxide with a perovskite-type lattice. With a $5d^1$ electronic

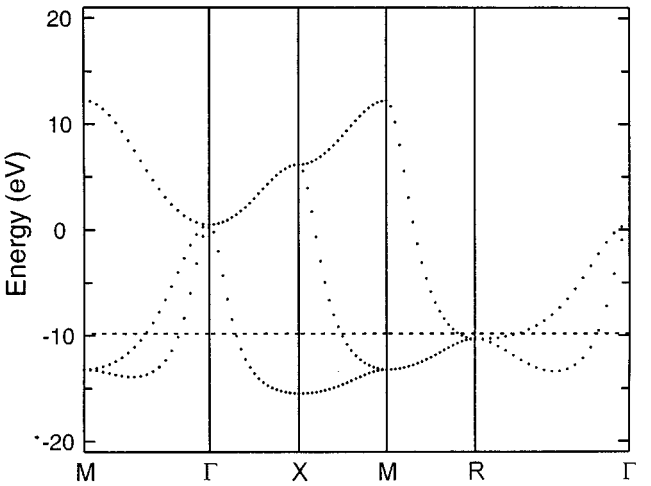


**FIG. 7.** Dispersion relations of the bands of the simple cubic P structure calculated with only *p* orbitals within the extended Hückel approximation. The dashed line refers to a Fermi level for a $p^3$ electron configuration.

configuration, the Fermi level lies near the bottom of the $t_{2g}$-block bands of $ReO_3$ (33). Its Fermi surfaces consist of two spheres of electron pockets centered at Γ and outside of these a cross of three perpendicular circular pipes. $ReO_3$ is a normal metal and does not exhibit any structural phase transition or electrical anomaly in the temperature region studied experimentally (34).

From the absence of Fermi surface nesting found in our calculations, we conclude that the phosphorus structure—either A17 or A7 under intermediate pressure—should not be considered as a structure distorted from a simple cubic lattice as a consequence of a Peierls instability. Instead, we suggest that the origin of the distortion is the *s*–*p* mixing, a more local effect.

To understand the effect of *s*–*p* mixing on the phosphorus structure, we might first consider a simpler example. It is well known that strong *s*–*p* mixing is responsible for the tetrahedral geometry in group 14 elements such as C, Si, and Ge (35). Given one more electron at each site, their four-coordinate environment cannot be suitable for P, since the extra electron would then enter the high-lying σ* antibonding bands. A more stable (isoelectronic) structure can be generated by cutting one bond around each site. A σ* band of the original tetrahedrally bonded lattice is then lowered, becomes nonbonding, and accommodates the extra electron to produce a lone pair at each site. Thus, given the existence of strong *s*–*p* mixing and this electron count, lone pair formation is essential for a stable structure, and each site is three-coordinate.

Something similar may occur in simple cubic P on transforming to an A7 structure as the applied pressure decreases. In its simple cubic form, the filled part of the *p* bands is antibonding between *s* and *p* orbitals. By breaking bonds and forming a lone pair at each site, this antibonding component is diminished in the filled bands. The resultant symmetry lowering allows the *s* and *p* orbitals to mix more effectively. Thus, the bonding character in the filled part of the bands becomes enhanced, and the P–P bond distance in the layer decreases significantly. Meanwhile, the unfilled part of the *p* bands is strongly destabilized by the enhanced antibonding and is pushed above the Fermi level (36) (Scheme 7).

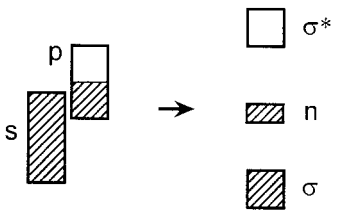


**Scheme 7**

However, the A7 structure does not seem to provide sufficient room to accommodate the newly formed lone pairs of phosphorus. A band gap between nonbonding and antibonding bands still does not open, and the system is semimetallic. Under lower pressure, phosphorus takes on an A17 structure, whose density is lower than that of the A7 (37). The band gap finally opens, resulting in a semiconductor.

## HEAVIER GROUP 15 ELEMENTS

As one moves down group 15, *p* orbitals become more diffuse and their interactions are weaker. In contrast, the *s* orbitals become compact and their energies decrease, due to the relativistic effect (38, 39). As a result, *s*–*p* mixing decreases drastically on going down a group in the periodic table. The extended Hückel parameters are nonrelativistic, and our calculational method does not cope with spin–orbit coupling, another manifestation of the relativistic effect.

The LAPW band structure calculation for simple cubic As by Mattheiss *et al.* shows that the *s* band lies rather low and is less dispersive (22). At *R* the energy of the *s* band is lower than those of the *p* bands. However, it is still higher than the lowest energy of the *p* bands (at *X*); that is, the *s* and *p* bands still overlap. There is no strong band repulsion, because there is no band crossing between the *s* and *p* bands. Strikingly, the overall features of the *p* bands are quite similar to the Hückel calculations shown in Fig. 5. One important difference in Mattheiss *et al.*'s results is a relatively small band splitting occurring along $\Gamma \rightarrow M$ and $\Gamma \rightarrow R$. This band-splitting feature is similar to what is found in the extended Hückel calculation with only *p* orbitals (shown in Fig. 7). Unfortunately, the authors did not calculate Fermi surfaces. From the band structure, however, we expect that the Fermi surfaces are in shape between Figs. 5 and 7. In

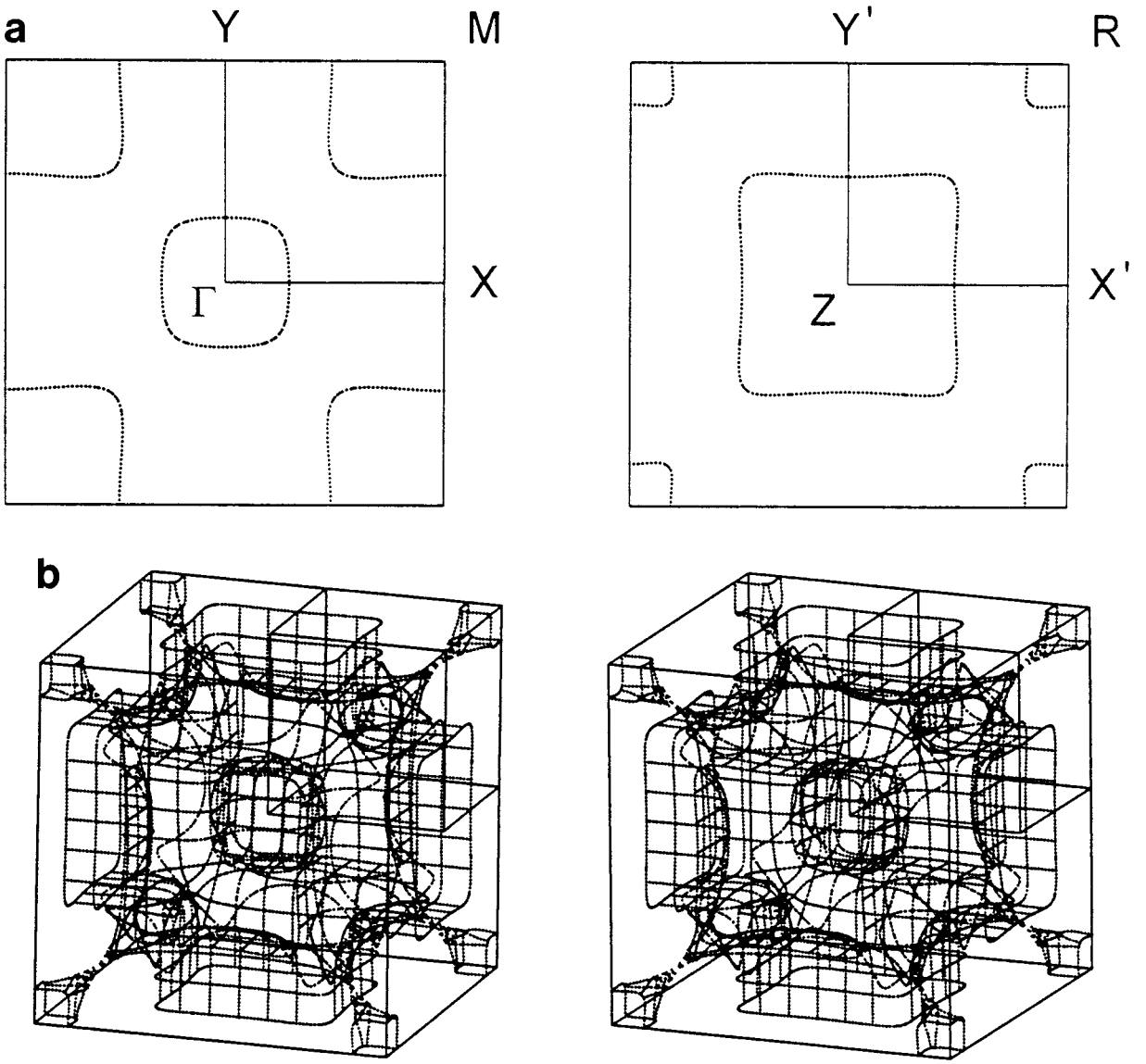


**FIG. 8.** The Fermi surfaces from the band structure of Fig. 7 in (a) cross-section views on the planes of $k_z = 0$ and $0.5\mathbf{c}^*$ and in (b) a perspective stereoview.

simple cubic As, therefore, we would expect better Fermi surface nesting than what we found in Fig. 8, but still imperfect.

Although in simple cubic As the *s–p* mixing is not as strong as in simple cubic P, it should be still considered as an important contributor to the distortion. Indirect evidence for this can be found in the behavior of GeTe under pressure (41). In a St. John–Bloch plot, GeTe lies very close to Sb and As, implying that its structural behavior will be similar to Sb and As (19, 20). At ambient pressure, GeTe has a rhombohedral structure like As (as well as Sb and Bi), and is a narrow-gap semiconductor. Upon increasing the pressure, GeTe transforms to a NaCl-type structure (i.e., an ordered simple cubic structure) around 3GPa. The resisitivity decreases monotonically to about 6GPa and does not exhibit any anomaly during the phase transformation. Band calculations also support the semiconducting nature of GeTe in its cubic form (41b). The implication is that the transformation has nothing to do with a Peierls instability, but with the *s–p* mixing.

As mentioned earlier, *s–p* mixing and Peierls distortion cause the same type of distorted local geometries in group 15 elements. In principle, *s–p* mixing can occur whether the Fermi surfaces are nested or not. How much it actually contributes to the distortion depends on the magnitude of the *s–p* interactions. For Sb and Bi, the role of the *s* orbital

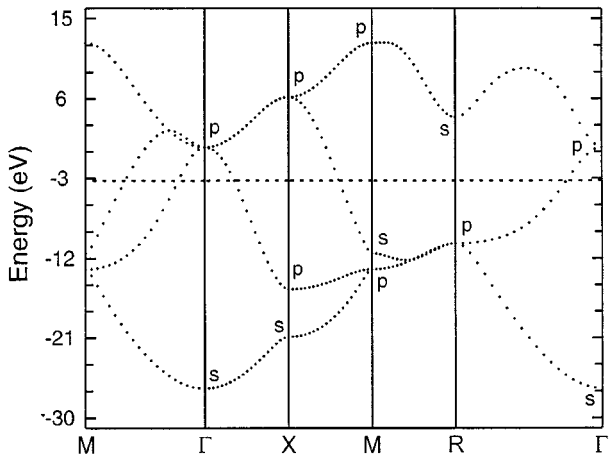


**FIG. 9.** Dispersion relations of the bands of the simple cubic P structure within the extended Hückel approximation. The dashed line refers to a Fermi level for a $s^2p^3$ electron configuration.

in chemical bonding becomes reduced, and the distortion due to the *s–p* mixing should be less severe. This explains why the distortion decreases in the order of P > As > Sb > Bi. We believe that the reverse order is predicted from considerations of the Peierls instability. On going down the periodic table, the Fermi surfaces are more likely to be nested. The Peierls instability should lead to least distortion in P. This is opposite to the experimental observation. A detailed examination of this trend, from a different perspective and in the context of normal and hypervalent geometries of group 15 and 16 extended structures, is given in a forthcoming study from our group by G. Papoian (40).

## CONCLUDING REMARKS

The band structure and Fermi surfaces of simple cubic P structure were calculated with the extended Hückel

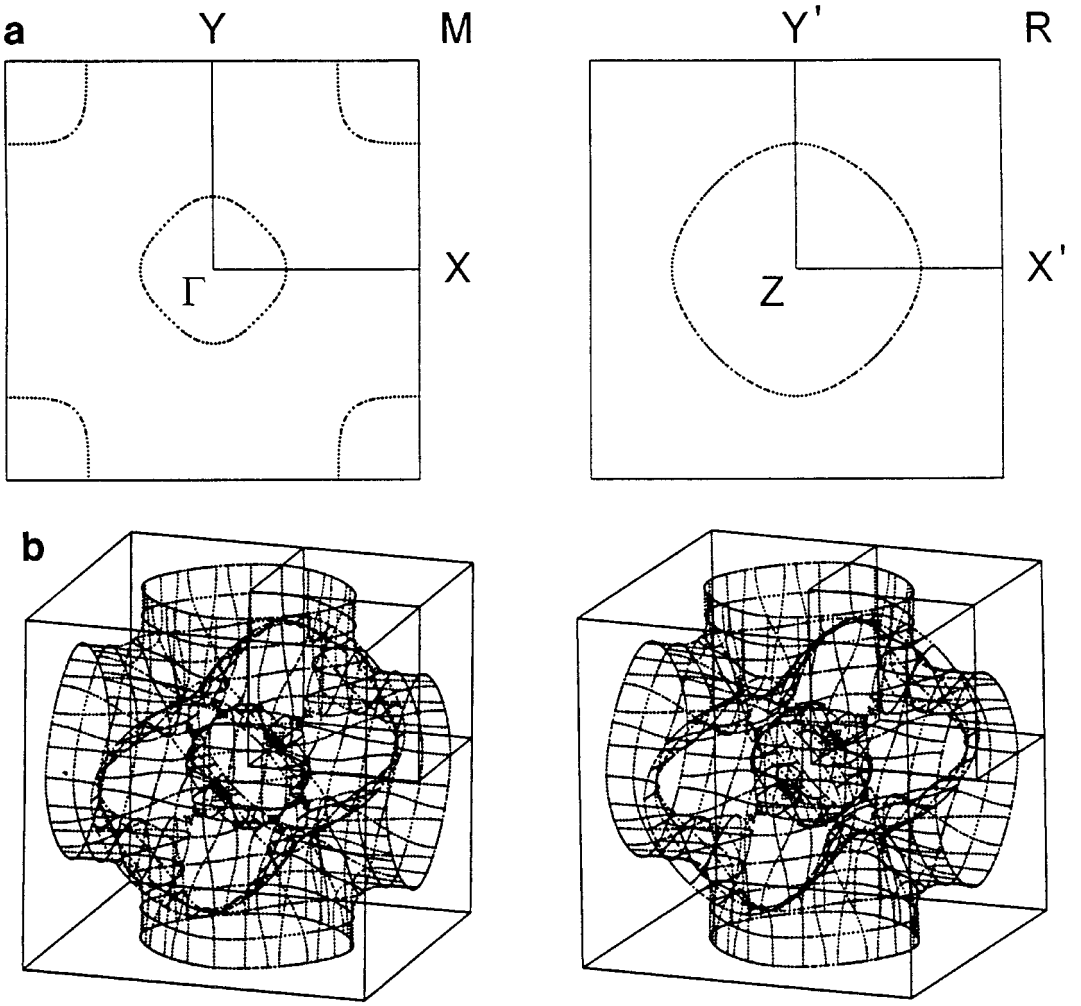


**FIG. 10.** The Fermi surfaces from the band structure of Fig. 9 in (a) cross-section views on the planes of $k_z = 0$ and 0.5**c*** and in (b) a perspective stereoview.

tight-binding method. The Fermi surfaces consist of a small sphere centered at Γ and a cross formed by three circular pipes perpendicular to each other. The *s* band is quite broad and overlaps with the *p* bands. The *s*–*p* mixing is significant and strongly affects the band structure and the shapes of the Fermi surfaces. The calculated Fermi surfaces are *not* nested. Within the simple Hückel approximation, the $p_\pi$ interaction severely deforms the ideal 1D Fermi surfaces. In reality, additional interactions, such as long-range and *s*–*p* interactions, destroy the Fermi nesting completely.

The unnested Fermi surfaces of simple cubic P structure argue strongly that the Peierls instability is not responsible for A17 and intermediate A7 structures of phosphorus as well as its transformation to a simple cubic structure under pressure. We suggest that the *s*–*p* mixing stabilizes the local distorted geometry in black phosphorus, by forming a nonbonding lone pair band. The *s*–*p* mixing should decrease down the group due to the *s*-orbital contraction. This explains why the distortion is the largest in black phosphorus. The strongest *s*–*p* mixing occurs in P, driving the largest distortion, even though the Fermi surface nesting is absent in its simple cubic form. For the heavier group 15 elements, the Fermi surfaces are more likely to be nested, especially due to the weaker *p* orbital interactions and the smaller involvement of *s* orbitals in chemical bonding.

## ACKNOWLEDGMENTS

D.-K. S. thanks Prof. M.-H. Whangbo for kindly providing the CAESAR program for this study. We appreciate helpful discussions with G. Papoian. We are also grateful to the National Science Foundations for its support of our research through Grant CHE 9408455.

## REFERENCES

1. R. E. Peierls, "Quantum Theory of Solids." Oxford University Press, London, 1955.
2. T. A. Albright, J. K. Burdett, and M.-H. Whangbo, "Orbital Interactions in Chemistry." Wiley, New York, 1985.
3. R. Hoffmann, "Solids and Surfaces." VCH, New York, 1988.
4. (a) K. Motizuki (Ed.), "Structure Phase Transitions in Layered Transition Metal Compounds," Reidel, Dordrecht, The Netherlands, 1986. (b) E. Doni and R. Girlanda, in "Electronic Structure and Electronic Transitions in Layered Materials" (V. Grasso, Ed.), p. 1. Reidel, Dordrecht, The Netherlands, 1986.
5. E. Canadell and M.-H. Whangbo, *Chem. Rev.* **91,** 1034 (1991).
6. M.-H. Whangbo and E. Canadell, *J. Am. Chem. Soc.* **114,** 9587 (1992).
7. C. Schlenker, J. Dumas, M. Greenblatt, and S. van Smaalen (Eds.), "Physics and Chemistry of Low-Dimensional Inorganic Conductors." Plenum, New York, 1996.
8. Grüner, "Density Waves in Solids." Addison-Wesley, Reading, MA, 1994.
9. M. Greenblatt, *Acc. Chem. Res.* **29,** 219 (1996).
10. J. K. Burdett and S. Lee, *J. Am. Chem. Soc.* **105,** 1079 (1983).
11. H. A. Jahn and E. Teller, *Proc. R. Soc. London, Ser. A* **161,** 220 (1937).
12. For recent reviews, see (a) M. Greenblatt, *Int. J. Mod. Phys. B* **7,** 3937 (1993), (b) P. Four and J.-P. Pouget, *Int. J. Mod. Phys. B* **7,** 3973 (1993), (c) E. Canadell and M.-H. Whangbo, *Int. J. Mod. Phys. B* **7,** 4005 (1993), (d) J. Dumas and C. Schlenker, *Int. J. Mod. Phys. B* **7,** 4045 (1993), (e) J.-P. Pouget, in "Low-Dimensional Electronic Properties of Molybdenum Bronzes and Oxides" (C. Schlenker, Ed.), p. 87, Kluwer, Dordrecht, The Netherlands, 1989, (f) C. Schlenker, J. Dumas, C. Escribe–Filippini, and H. Guyot, *ibid*., p. 159, (g) M. Greenblatt, *ibid*, p. 1. (h) R. M. Fleming and R. J. Cava, *ibid*., p. 259, (i) M. Greenblatt, *Chem. Rev.* **88,** 31 (1988), and (j) C. Schlenker, J. Dumas, C. Escribe-Filippini, H. Guyot, J. Marcus, and J. Fourcadot, *Philos. Mag. B* **52,** 643 (1985).
13. Sometimes, CDW materials still remain metallic after structural distortion, showing a metal-to-metal transition. This can be due to incomplete Fermi surface nesting. Or, bands may still overlap when the distortion is weak. As can be seen later, this explains why black phosphorus is semiconducting, while the heavier elements in group 15 are semimetallic. Compared to black phosphorus, As, Sb, and Bi have much weaker distortions, thereby exhibiting (small) band overlapping.
14. M.-H. Whangbo, D.-K. Seo, and E. Canadell, *in* "Physics and Chemistry of Low-Dimnsional Inorganic Conductors" (C. Schlenker, J. Dumas, M. Greenblatt, and S. van Smaalen, Eds.), p. 285. Plenum, New York, 1996, the references therein.
15. (a) A. Brown and S. Rundqvist, *Acta Crystallogr.* **19,** 684 (1965). (b) D. Schiferl and C. S. Barrett, *J. Appl. Crystallogr.* **2,** 30 (1969). (c) C. S. Barrett and P. Cucka, *Acta Crystallogr.* **16,** 451 (1963). (d) P. Cucka, C. S. Barrett, and P. Cucka, *Acta Crystallogr.* **15,** 865 (1962).
16. (a) J. Donahue, "The Structures of the Elements." Wiley, New York, 1974. (b) U. Müller, "Inorganic Structural Chemistry." Wiley, Chichester, England, 1993.
17. In the intermediate pressure region between $\sim$5 and $\sim$12 GPa, black phosphorus has a A7 type structure and is semimetallic. At around 10 GPa, the ratio of nonbonded and bond distances is 1.54, still the largest among the group 15 elements. The P–P bond distance within the layer is 2.13 Å.
18. (a) J. C. Jamieson, *Science* **139,** 1291 (1963). (b) J. Wittig and B. T. Mattias, *Science* **160,** 994 (1968). (c) M. Okajima, S. Endo, Y. Akahama, and S. Narita, *Japan. J. Appl. Phys.* **23,** 15 (1984). (d) L. F. Vereschchagin and S. S. Kabalkina, *Soviet Phys. JETP* **20,** 274 (1964).
19. P. B. Littlewood, *J. Phys. C* **13,** 4855 (1980).
20. P. B. Littlewood, *CRC Crit. Rev. Solid State Mater. Sci.* **11,** 229 (1983).
21. R. J. Needs, R. M. Martin, and O. H. Nielsen, *Phys. Rev. B* **33,** 3778 (1986).
22. L. F. Mattheiss, D. R. Hamann, and W. Weber, *Phys. Rev. B* **34,** 2190 (1986).
23. T. Sasaki, K. Shindo, K. Niizeki, and A. Morita, *Solid State Commun.* **62,** 795 (1987).
24. M. H. Cohen, L. M. Falicov, and S. Golin, *IBM J. Res. Develop.* **8,** 215 (1964).
25. The participation of lower fully occupied *d* orbitals is even more unlikely, so that these orbitals remain practically unchanged. See, for example, (a) X. Gonze, J.-P. Michenaud, and J.-P. Vigneron, *Phys. Rev. B* **41,** 11827 (1990), (b) J. H. Xu, E. G. Wang, C. S. Ting, and W. P. Su, *Phys. Rev. B* **48,** 17271 (1993), and (c) G. Jezequel, J. Thomas, and I. Pollini, *Phys. Rev. B* **56,** 6620 (1997). Upper empty *d* orbitals might contribute, especially for the heavier elements. However, the amount of such mixing is small and can be neglected judging from the band structures of those elements. See, for example, Refs. (21), (22), (25a), and (25b).
26. J.-P. Gaspard, A. Pellegatt, F. Marinelli, and C. Bichara, *Philos. Mag. B* **77,** 727 (1998).
27. R. Hoffmann, *J. Chem. Phys.* **39,** 1397 (1963).
28. M.-H. Whangbo and R. Hoffmann, *J. Am. Chem. Soc.* **100,** 6093 (1978).

29. J. Ren, W. Liang, and M.-H. Whangbo, "Crystal and Electronic Structure Analyzer (CAESAR)," North Carolina State University, Raleigh, NC, 1998.
30. E. Clementi and C. Roetti, *At. Data Nucl. Data Tables* **14,** 177 (1974).
31. (a) M.-H. Whangbo, *in* "Crystal Chemistry and Properties of Materials with Quasi-One Dimensional Structures" (J. Rouxel, Ed.), p. 27, Reidel, Dordrecht, The Netherlands, 1986. (b) K. Yoshizawa and R. Hoffmann, *J. Chem. Phys.* **103,** 2126 (1995). (c) D.-K. Seo and R. Hoffmann, in preparation.
32. Γ and *M* are high-symmetry **k**-points where three and two *p* bands are degenerate, respectively. Although $p_x + p_y$ and $p_x - p_y$ do not need to be the correct linear combinations at these point, we chose Γ and *M*, where the crystal orbitals are real, to illustrate the characters of the crystal orbitals at the low-symmetry points along $\Gamma \rightarrow M$. The same viewpoint is taken in the subsequent discussions on the crystal orbital characters along $\Gamma \rightarrow R$.
33. (a) P. A. Cox, "Transition Metal Oxides." Oxford University Press, New York, 1992. (b) L. F. Mattheiss, *Phys. Rev.* **181,** 987 (1969). (c) L. F. Mattheiss, *Phys. Rev. B* **2,** 3918 (1970).
34. S. M. Marcus, *Phys. Lett.* **27A,** 584 (1968).
35. (a) W. A. Harrison, "Electronic Structure and the Properties of Solids," Freeman, San Francisco, 1980. (b) P. A. Cox, "The Electronic Structure and Chemistry of Solids." Oxford University Press, New York, 1991. (c) D. Pettifor, "Bonding and Structure of Molecules and Solids," Clarendon Press, Oxford, England, 1995.
36. The earlier studies of Burdett and his coworkers also pointed to the importance of lone pair formation in stabilizing A17 and A7 structures. See J. K. Burdett, P. Haaland, and T. J. McLarnan, *J. Chem. Phys.* **75,** 5774 (1981).
37. E. Parthê, *Z. Kristallogr.* **115,** 52 (1961).
38. (a) K. S. Pitzer, *Acc. Chem. Res.* **12,** 271 (1979). (b) P. Pykkö, *Acc. Chem. Res.* **12,** 276 (1979). (c) L. L. Lohr and P. Pykkö, *Chem. Phys. Lett.* **62,** 333 (1979). (d) S. Lee and B. Foran, *J. Am. Chem. Soc.* **116,** 154 (1994).
39. Even without relativistic effect, the *s* orbital is slightly more contracted compared to the *p* orbitals in the same shell. This effect is enhanced as going down the group 15. See, for example, Ref. (40).
40. G. Papoian and R. Hoffmann, in preparation.
41. (a) L. G. Khvostantsev, V. A. Sidorov, L. E. Shelimova, and N. Kh. Abrikosov, *Phys. Stat. Sol.* (*a*) **74,** 185 (1982). (b) K. M. Rabe and J. D. Joannopoulos, *Phys. Rev. B* **36,** 3319 (1987). (c) A. Onodera, I. Sakamoto, Y. Fujii, N. Môri, and S. Sugai, *Phys. Rev. B* **56,** 7935 (1997).